Clinics of Oncology

Review Article

ISSN: 2640-1037 | Volume 6

Combination of Short Chain Fatty Acid Butyrate and Ferroptosis Inducer for the Inhibition of Colon Cancer via Enhancing Ferroptosis

Zhen L*

State Key Laboratory of Pharmaceutical Biotechnology, School of Life Sciences, Nanjing University, China

***Corresponding author:**

Li Zhen,

State Key Laboratory of Pharmaceutical Biotechnology, School of Life Sciences, Nanjing University, No.163 Xianlin Road, Nanjing, 210023, China

Received: 10 June 2023

Accepted: 26 July 2023

Published: 04 Aug 2023

J Short Name: COO

Keywords:

Colon cancer cell line; Short chain fatty acid; Fluorescent imaging; Enhancing ferroptosis

Citation:

Zhen L, Combination of Short Chain Fatty Acid Butyrate and Ferroptosis Inducer for the Inhibition of Colon Cancer via Enhancing Ferroptosis. Clin Onco. 2023; 6(25): 1-8

1. Abstract

Herein, short chain fatty acid butyrate was introduced as an important auxiliary agent to combine with ferroptosis inducer for enhancing the ferroptosis in the inhibition of colon cancer. It was found that butyrate could not induce the ferroptosis independently, whereas the combination of butyrate and ferroptosis inducer (Erastine or Sorafenib) could enhance the extent of ferroptosis. The affected indexes included the iron accumulation, oxidative damage to lipids, the expression of GPX4, a key antioxidant enzyme, as well as the morphological characteristics under scrutiny. Via enhancing ferroptosis, the combination of butyrate and ferroptosis inducer could effectively inhibit the growth of colon cancer cell line HCT116. Moreover, butyrate plus Erastine was a better pair than Butyrate plus Sorafenib in aggravating the ferroptosis process. This work raised possible approaches for treating colon cancer via enhancing ferroptosis.

2. Introduction

Colon carcinoma is a prevalent malignant tumor of the gastrointestinal tract, characterized by inconspicuous early symptoms and severe systemic manifestations in advanced stages, including anemia, weight loss, bloody stool, and diarrhea [1-4]. Among digestive system malignancies, colon cancer ranks second in terms of incidence and mortality rates, following gastric cancer, esophageal cancer, and primary liver cancer [5]. Despite its prevalence, the precise mechanisms underlying colon cancer remain unclear. The majority of colon cancer cases are adenocarcinomas, with a few instances of squamous cellular or mucinous carcinoma, posing challenges for effective treatment due to their ability to metastasize via lymph and blood circulation [6]. Consequently, the focus of colon cancer treatment has shifted towards understanding metabolism-related mechanisms, with particular interest in ferroptosis, given its strong association [7-9]. Ferroptosis, a newly discovered form of iron-dependent programmed cell death, differs from apoptosis, necrosis, and autophagy, exhibiting distinct morphological, biological, and mechanistic pathways. The intricate signaling pathways governing ferroptosis have been implicated in the development of various diseases [10-14]. Recent studies have identified several key indicators of ferroptosis, including levels of ferrous ions (Fe2+), glutathione (GSH), and glutathione peroxidase 4 (GPX4) [15]. Inducing ferroptosis in cancer cells using specific agents such as Sorafenib and Erastine represents a promising therapeutic strategy to overcome drug resistance and develop combination approaches. Monitoring molecular markers enables precise and controllable treatment modalities [13, 16-18]. However, given that current agents can only induce ferroptosis to a limited extent, there is a need for additional methods to enhance therapeutic approaches [19-23].

In this groundbreaking study, we explore the potential of short-chain fatty acids (SCFAs) as effective agents for enhancing ferroptosis in colon cancer when combined with a ferroptosis inducer. SCFAs are organic fatty acids with fewer than six carbon atoms in their molecular structure, including acetic acid, propionic acid, and

butyric acid [24, 25]. These SCFAs are produced by beneficial intestinal bacteria through the fermentation of dietary fiber and carbohydrates, and they play crucial roles in maintaining health and preventing diseases [25-29]. Butyric acid, a representative SCFA, serves as a vital energy source for colon cells. It provides over 90% of the total energy required by colon cells and helps maintain the integrity of the intestinal wall, preventing conditions such as intestinal fistulas and chronic inflammation [30-33]. By fulfilling the energy demands of colon cells, the reliance on aerobic glycolysis in tumor cells is significantly reduced, thereby increasing the metabolic pressure on tumor cell mitochondria. This leads to specific apoptosis of tumor cells and inhibition of tumor growth. In this study, we investigate the combination of butyrate, a short-chain fatty acid, with a ferroptosis inducer to inhibit colon cancer by enhancing ferroptosis, while closely monitoring the occurrence of ferroptosis [34-36]. This research sheds light on a novel approach that holds promise for developing effective therapies against colon cancer by harnessing the synergistic effects of SCFAs and ferroptosis inducers.

3. Experimental

The detailed experimental protocols of the cell culturing, cell imaging, flow cytometry assays, western blot analysis, transmission electron microscope (TEM) imaging, immunofluorescence staining, concentration determination, and cell survival rate assay were described in Supplementary Materials.

4. Results and Discussion

4.1. Determination of the Iron Overload

As we mentioned, that ferroptosis exhibits characteristics such as iron overload and lipid peroxidation, with key indicators including Fe2+ levels and GPX4 (Scheme 1). Therefore, the evaluation of the extent of ferroptosis should commence with the determination of iron overload. In this study, the HCT116 human colon cancer cell line was chosen for intracellular analysis. The cells were divided into six groups as follows: 1) Control; 2) Butyrate only; 3) Erastine only; 4) Sorafenib only; 5) Butyrate plus Erastine; 6) Butyrate plus Sorafenib. This grouping strategy was maintained throughout all subsequent experiments. To assess the Fe2+ levels, FeRhoNox-1 (an Fe2+ indicator) was utilized, while Hoechst (a nuclear dye for living cells) was employed to locate the living cells (Figure 1A & 1B). In the control group, the fluorescence signal of FeRhoNox-1 in the red channel was relatively weak. Treatment with Butyrate alone did not result in an increase in the signal, indicating that Butyrate alone could not induce ferroptosis. However, the addition of Erastine or Sorafenib independently led to a noticeable enhancement of the fluorescence signal in the red channel. Furthermore, when Butyrate was combined with Erastine or Sorafenib, the red fluorescence signal was further amplified. Hence, the combination of Butyrate with the ferroptosis inducers (Erastine or Sorafenib) resulted in higher Fe2+ levels, thereby increasing the iron overload in living colon cancer cells.

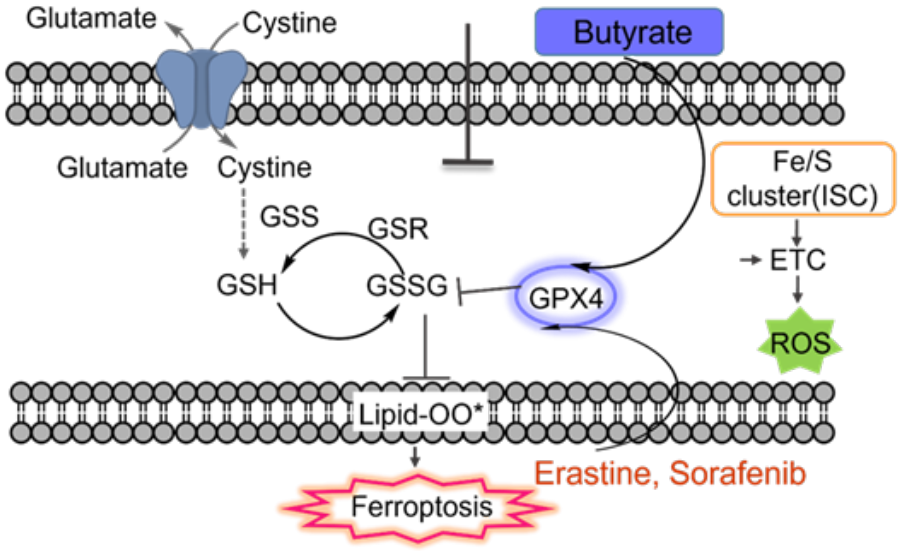

Scheme 1: The Classical Induction Mechanism of Ferroptosis.

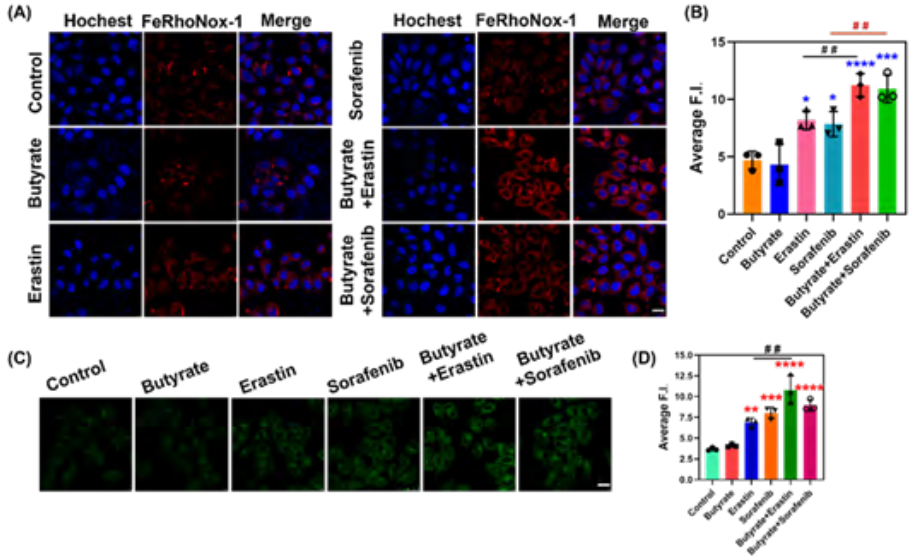

Figure 1: (A) Fluorescence microscopic images of the HCT116 cells. The cells were treated with 0.01% DMSO, Butyrate (500 μM), Erastine (10 μM), Sorafenib (10 μM), Butyrate (500 μM) with Erastine (10 μM), and Butyrate (500 μM) with Sorafenib (10 μM) in DMEM medium at 37 °C for 24 h. After being washed with PBS buffer for three times, the cells were cultured with FeRhoNox-1 dye (5 μM) for another 30 min. Then the cells were incubated with Hoechst for 15 min. Each group of the data had blue channel, red channel, and merged channel. The blue channel was collected with the excitation at 405 nm and the emissions from 430 to 480 nm, the red channel was collected with the excitation at 488 nm and the emissions from 560 to 620 nm. Scale bar: 25 μm. (B) Quantification of imaging data (A). n = 3, error bars were ± SD., Statistical analysis was performed with two-way ANOVA with multiple comparisons. The administration group was compared with the control group: ****p value < 0.0001, ***p value < 0.001, *p value < 0.05. The combined administration group was compared with the single administration group: ##p value < 0.01. (C) The cells were pretreated the same as (A). After being washed with PBS buffer for three times, the cells were cultured with DCFH-DA (10 μM) for another 30 min. Fluorescence images were collected the excitation at 405 nm and emissions from 500 to 560 nm. Scale bar: 25 μm. (D) Quantification of imaging data (c). n = 3, error bars were ± SD., Statistical analysis was performed with two-way ANOVA with multiple comparisons. The administration group was compared with the control group: ****p value < 0.0001, ***p value < 0.001, **p value < 0.01. The combined administration group was compared with the single administration group: ##p value < 0.01.

4.2. Determination of the lipid peroxidation

Subsequently, the feature of lipid peroxidation was checked. With the same division of groups, the generation of reactive oxygen species (ROS) was imaged by the incubation with DCFH-DA (a ROS indicator) with the fluorescence signal in the green channel (Figure 1C & 1D). The control and Butyrate-treated groups exhibited weak green fluorescence signals. The pre-treatment with Erastine or Sorafenib independently resulted in the remarkable enhancement of the fluorescence intensity, which meant that the ferroptosis inducers could lead to the generation of ROS. The combination of Butyrate and Erastine led to significant further increase of the green fluorescence signal, while the combination of Butyrate and Sorafenib showed the similar fluorescent intensity to that of the Sorafenib-only group. Thus, for enhancing the generation of ROS, Butyrate could merely cause further increase via the combination of Erastine rather than Sorafenib.

Afterwards, BODIPY C11 dye was selected to reflect the lipid peroxidation in a ratio (green/red) mode. The accumulation of ROS can be visualized as the fluorescence enhancement in the green channel as well as the intensity decrease in the red channel. The results were present as images and ratio values (Figure 2A & 2B). In the control and Butyrate-treated groups, there were weak signals in the green channel and relatively strong signals in the red channel, which indicated the low ROS level. In the groups treated with Erastine and Sorafenib, the fluorescence signals in the green channels exhibited a significant increase, approaching and nearly matching those observed in the red channels. Thus, the ferroptosis inducers independently caused the accumulation of ROS. The combination of Butyrate and each ferroptosis inducer could further increase the green/red ratio value. Therefore, on the basis of using ferroptosis inducer, the supplement of Butyrate could lead to further lipid peroxidation. In addition, compared with Sorafenib, Erastine was more suitable for the combination with Butyrate due to the larger increase of the green/red ratio value. The same cell groups were analyzed by FCM (flow cytometry) in APC-A channel (Red) and PE-A (Green) channels. In the two-dimensional map in Figure 2C, the results agreed with that of confocal images and quantification analysis.

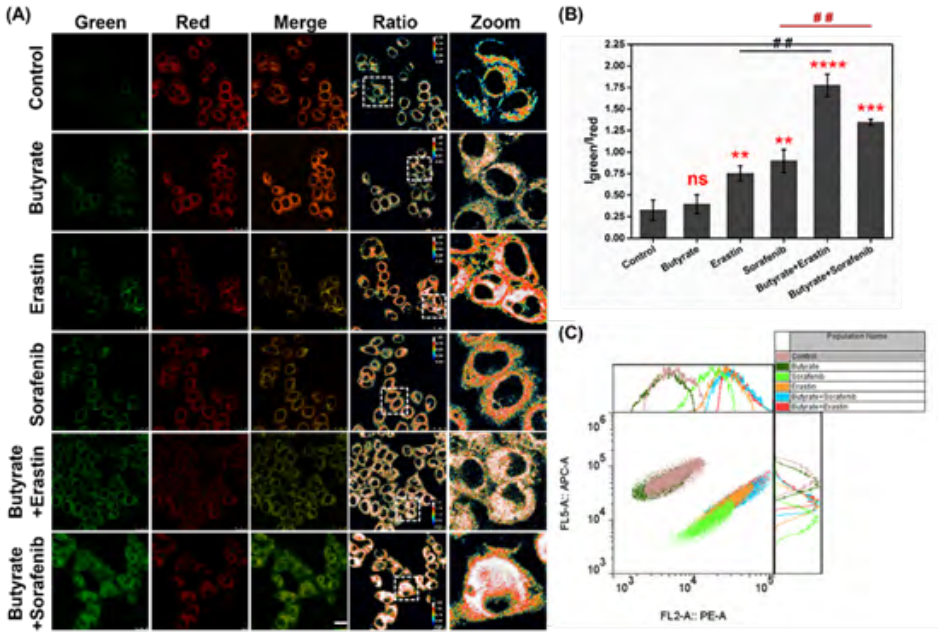

Figure 2: (A) Fluorescence microscopic images of the HCT116 cells. The cells were treated with 0.01% DMSO, Butyrate (500 μM), Erastine (10 μM), Sorafenib (10 μM), Butyrate (500 μM) with Erastine (10 μM), and Butyrate (500 μM) with Sorafenib (10 μM) in DMEM medium at 37 °C for 24 h. After being washed with PBS buffer for three times, the cells were cultured with BODIPY C11 dye (5 μM) for another 30 min. Each group of the data had green, red, merged, ratio and zoom channels. The green channel was collected with the excitation at 488 nm and the emissions from 500 to 550 nm; the red channel was collected with the excitation at 488 nm and the emissions from 580 to 630 nm, the ratio images were obtained from green channel/red channel. Scale bar: 25 μm. (B) Quantification of imaging data (A). n = 3, error bars were ± SD., Statistical analysis was performed with two-way ANOVA with multiple comparisons. ns meant not significantly different, the administration group was compared with the control group: ****p value < 0.0001, ***p value < 0.001, **p value < 0.01. The combined administration group was compared with the single administration group: ##p value < 0.01. (C) The cells were pretreated the same as (A). Then 20000 cells were collected by FCM (flow cytometry). Flow scatter diagram showed APC-A channel (Red) and PE-A (Green) channels.

4.3. Morphological observation of ferroptosis

After the determination of the two typical features of iron overload and lipid peroxidation, the morphological observation under transmission electron microscopy (TEM) was conducted to further confirm the extent of ferroptosis (Figure 3). Compared with the mitochondria morphology in the control group, there was no obvious variation in the Butyrate-treated group. However, in the other four groups, the mitochondria became smaller with more dense membrane structures, and there were fewer ridges. This result was consistent with the morphological characteristics of ferroptosis.

4.4. Determination of the GPX4 expression

Following the determination on the typical features in Fe2+, ROS and mitochondria morphology, the key enzymes in the process of ferroptosis, represented by GPX4, should be checked. Both the immunofluorescence staining analysis and western blot analysis were carried out. In the immunofluorescence staining analysis, the dye Alex488 with green fluorescence was added on the secondary antibody to image GPX4, while DAPI was used to show the location of the nucleus. The differences of the fluorescence intensity in the green channel were revealed by the confocal images (Figure 4A) as well as the quantification analysis (Figure 4B). In the control and Butyrate-treated groups, the notable fluorescence signals in the green channel suggested the normal GPX4 expression level. The treatment with Erastine or Sorafenib resulted in the decrease of the green fluorescence intensity, which indicated the down-regulation of GPX4 expression. Both the Butyrate with Erastine group and the Butyrate with Sorafenib group exhibited further decrease of the fluorescence signals in the green channel, compared with that of the ferroptosis inducer-treated groups without Butyrate. Moreover, the Butyrate with Erastine group showed the weakest fluorescence intensity. This result once again verified that the addition of Butyrate could enhance the induction effect of ferroptosis inducer.

On the other hand, the GPX4 expression level was checked by western blot analysis (Figure 4C & 4D). As seen in the stripes and quantification analysis, the results agreed with that of the immunofluorescence staining analysis. Therefore, by measuring the GPX4 level, the auxiliary effect of Butyrate on the ferroptosis inducers was convinced.

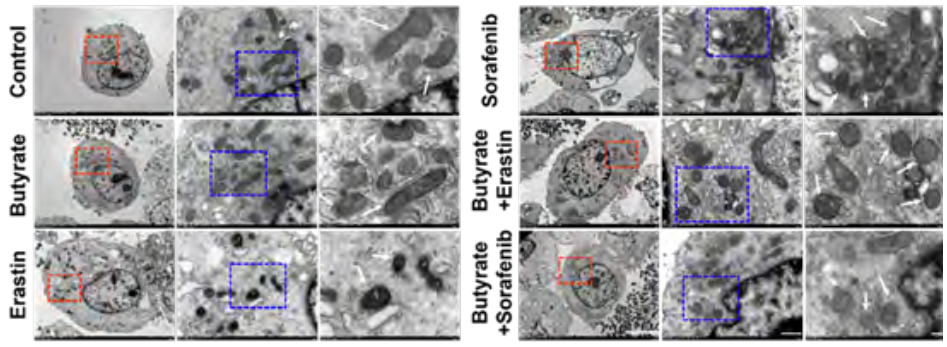

Figure 3: Transmission electron microscopy of the HCT116 cells. The cells were pretreated with 0.01% DMSO, Butyrate (500 μM), Erastine (10 μM), Sorafenib (10 μM), Butyrate (500 μM) with Erastine (10 μM), and Butyrate (500 μM) with Sorafenib (10 μM) in DMEM medium at 37 °C for 24 h. The cell samples were prepared according to the procedure, sliced and then observed by the electron microscope. The white arrowheads indicated where the shape of the mitochondria and ridges change. Scale bar: 2 μm, 1 μm, 500 nm.

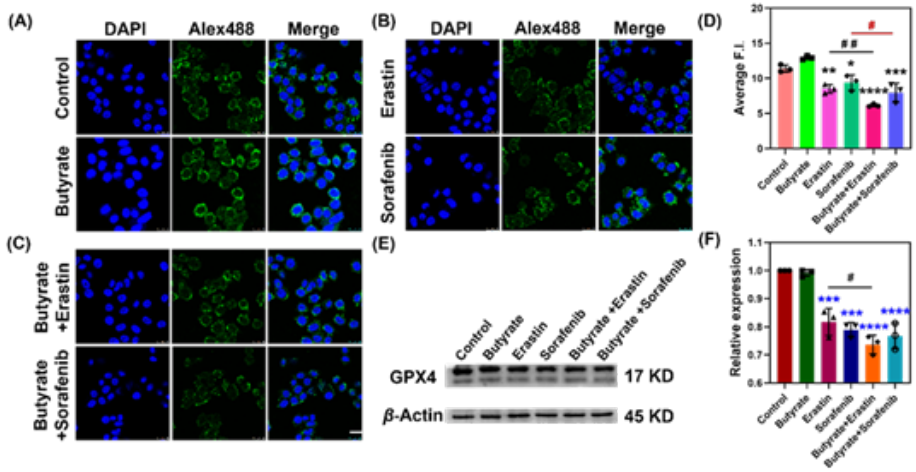

Figure 4: (A) Immunofluorescence imaging of the HCT116 cells. The cells were pretreated with 0.01% DMSO, Butyrate (500 μM), Erastine (10 μM), Sorafenib (10 μM), Butyrate (500 μM) with Erastine (10 μM), and Butyrate (500 μM) with Sorafenib (10 μM) in DMEM medium at 37 °C for 24 h. Then the cells were immobilized and permeated. Immunofluorescence staining analysis of GPX4 was conducted. A secondary antibody labeled with Alex488 was incubated. The fluorescence images were collected with the excitation at 488 nm and the emissions from 500 to 560 nm. Scale bar: 25 μm. (B) Quantification of imaging data (A). n = 3, error bars were ± SD., Statistical analysis was performed with two-way ANOVA with multiple comparisons. The administration group was compared with the control group: ****p value < 0.0001, ***p value < 0.001, **p value < 0.01, **p value < 0.01. The combined administration group was compared with the single administration group: ##p value < 0.01, #p value < 0.05. (C) Western blot analysis of GPX4 in the HCT116 cells (the cells were pretreated the same as (A)). (D) Quantification of western blot analysis (E). Statistical analysis was performed with two-way ANOVA with multiple comparisons. The administration group was compared with the control group: ****p value < 0.0001, ***p value < 0.001. The combined administration group was compared with the single administration group: #p value < 0.05.

4.5. Other Indexes and Cell Viability

On the complement indexes of the ferroptosis induction, other indexes including GSH, superoxide dismutase (SOD) and LPO levels were also evaluated. Regulated by GPX4, the GSH level usually decreases during ferroptosis. In Figure 5A, the GSH level of each group was illustrated. Compared with the control group (~60 μg/mL), the Butyrate-treated group suggested no significant variation on the GSH level (~55 μg/mL). In the Erastine-treated and Sorafenib-treated groups, the GSH level decrease to about half of that of the control group (35-40 μg/mL). With the combination of Butyrate, the treatment of the ferroptosis inducers could achieve lower GSH levels in HCT116 cells (< 30 μg/mL). Typically, the combination of Butyrate and Erastine cause a GSH level as low as almost 20 μg/mL. This result agreed with that of the GPX4 determination. Meanwhile, the SOD level was shown in Figure 5B. The control group showed a SOD level of ~90 U/mL. The Butyrate-treated group indicated no significant difference. Either treated with Erastine or Sorafenib led to obvious decrease of the SOD level to ~80 U/mL. Additionally, the combination of Butyrate and the ferroptosis inducer resulted in further decrease of the SOD level to ~60 U/mL. For this index, the Butyrate plus Erastine group and the Butyrate plus Sorafenib group did not show obvious difference. On the contrary of the reductive indexes such as GSH and SOD, the oxidative index was also tested directly in spite of the imaging results. In the control and Butyrate-treated groups, the LPO (MDA) levels were quite low (~0.1 nmol/mL). The treatment

with Erastine or Sorafenib resulted in remarkable enhancement (3-5 folds) of the LPO level. Based on the level induced by the ferroptosis inducers (Erastine or Sorafenib), the combination with Butyrate could lead to a further increase of the LPO level to almost two folds (~0.7 nmol/mL).

Finally, after the fully confirmation of ferroptosis, the inhibition of colon cancer was investigated to discover whether the enhancement of ferroptosis by combining Butyrate could improve the anti-cancer effect. After the treatment according to the group division, the cell viability of HCT116 cells was measured (Figure 5D & S6). Basically, all the groups involving ferroptosis (treated by Erastine only, Sorafenib only, Butyrate plus Erastine, and Butyrate plus Sorafenib) indicated the inhibition of the cell growth in a dose-dependent manner. At each concentration of the ferroptosis inducer, no matter Erastine or Sorafenib, the combination with Butyrate caused a lower cell viability. Accordingly, the inhibition of colon cancer cell line was positively related to the induction of ferroptosis. Therefore, the combination of Butyrate towards the ferroptosis inducers could lead to more potent inhibition effect on colon cancer cells.

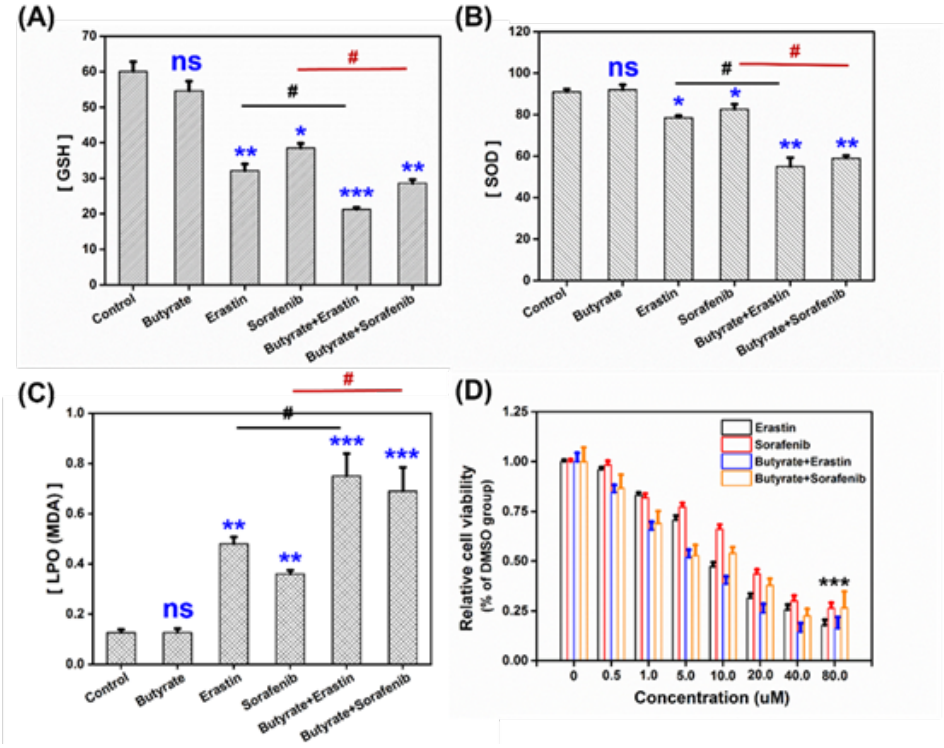

Figure 5: (A-C) Total GSH、SOD、LPO content in cells. The HCT116 cells were pretreated with 0.01% DMSO, Butyrate (500 μM), Erastine (10 μM), Sorafenib (10 μM), Butyrate (500 μM) with Erastine (10 μM), and Butyrate (500 μM) with Sorafenib (10 μM) in DMEM medium at 37 °C for 24 h. After the cells were collected, the cells were broken, and the supernatant of the cells was collected by the centrifugation. The test was conducted in strict accordance with the relevant kit methods. Statistical analysis was performed with two-way ANOVA with multiple comparisons. ***p<0.001, **p<0.01, *p<0.05, ns: no significant difference. (D) The HCT116 cells were incubated with various concentrations of Erastin (0, 0.5, 1.0, 5.0, 10.0 20.0, 40.0, 80.0 μM), Sorafenib (0, 0.5, 1.0, 5.0, 10.0 20.0, 40.0, 80.0 μM), Butyrate (500 μM) with Erastine, and Butyrate (500 μM) with Sorafenib.

5. Conclusion

To sum up, in this work, Butyrate (representing SCFAs) was introduced as an important auxiliary agent to combine with ferroptosis inducer for enhancing the ferroptosis in the inhibition of colon cancer. The ferroptosis process was checked through the determination of iron overload, lipid peroxidation, GPX4 expression, and the morphological observation. The inhibition of the colon cancer cell line HCT116 was confirmed with the cell viability. The results revealed that Butyrate could not induce the ferroptosis independently, whereas the combination of Butyrate and ferroptosis inducer (Erastine or Sorafenib) could enhance the extent of ferroptosis from that of ferroptosis inducer-treated groups. Butyrate plus Erastine was a better pair than Butyrate plus Sorafenib in aggravating the ferroptosis process. The information in this work might be helpful for exploiting therapeutical approaches on treating colon cancer by enhancing the ferroptosis extent with the combination of auxiliary agent and ferroptosis inducers. The successful combination of butyrate and ferroptosis inducers to enhance ferroptosis and inhibit colon cancer opens up promising avenues for further research and potential clinical applications.

References

1. Golder AM, Pennel KA, Mansouri D, Horgan PG, Roxburgh CS, Biankin AV, et al. The association between tumour sidedness, clinicopathological characteristics and outcomes in patients undergoing curative resection for colon cancer, American Society of Clinical Oncology. 2022; 40: 148.
2. Wu J, Yeung SCJ, Liu S, Qdaisat A, Jiang D, Liu W, et al. Cyst (e) ine in nutrition formulation promotes colon cancer growth and chemoresistance by activating mTORC1 and scavenging ROS, Signal transduction and targeted therapy. 2021; 6(1): 188.
3. Calogero A, Cirillo M, Gennarelli N, Maio N, Buonomo N, Lobello R. P-0192 Cancer Colon Test: Evolution and Prospects in Colorectal Cancer Screening, Annals of Oncology. 2012; 23: iv85.
4. Garbe J, Rosendahl J, Krug s. Diarrhea associated with sigmoid cancer–as usual?, Gastroenterology. 2023; 2: 37.
5. Sung H, Ferlay J, Siegel RL, Laversanne M, Soerjomataram I, Jemal A, et al. Global cancer statistics 2020: GLOBOCAN estimates of incidence and mortality worldwide for 36 cancers in 185 countries, CA: a cancer journal for clinicians. 2021; 71(3): 209-49.
6. Burt RW, Cannon JA, David DS, Early DS, Ford JM, Giardiello FM, et al. Colorectal cancer screening, Journal of the National Comprehensive Cancer Network. 2013; 11(12): 1538-75.
7. Luo W, Dai W, Li Q, Mo S, Han L, Xiao X, et al. Ferroptosis-associated molecular classification characterized by distinct tumor microenvironment profiles in colorectal cancer. International Journal of Biological Sciences. 2022; 18(5): 1773.
8. Yan H, Talty R, Johnson CH. Targeting ferroptosis to treat colorectal cancer. Trends in Cell Biology. 2022; 33: 185-8.
9. Wang J, Millstein J, Arai H, Battaglin F, Kawanishi N, Jayachandran P, et al. The role of genetic variants involved with ferroptosis regulator genes in predicting outcomes in patients (pts) with RAS-mutant metastatic colorectal cancer (mCRC): Data from MAVERICC and TRIBE trials, American Society of Clinical Oncology. 2022; 40: 197.
10. Wang ZL, Yuan L, Li W, Li JY. Ferroptosis in Parkinson's disease: glia–neuron crosstalk, Trends in Molecular Medicine. 2022; 28(4): 258-69.
11. Bayır H, Dixon SJ, Tyurina YY, Kellum JA, Kagan VE. Ferroptotic mechanisms and therapeutic targeting of iron metabolism and lipid peroxidation in the kidney, Nature Reviews Nephrology. 2023; 1-22.
12. Ru Q, Li Y, Xie W, Ding Y, Chen L, Xu G, et al. Fighting age-related orthopedic diseases: focusing on ferroptosis, Bone Research. 2023; 11(1): 12.
13. Zhang JB, Tong J, Sun DY, Fu JT, Li DJ, Wang P. Targeting ferroptosis in cardio-metabolic-diseases: Mechanisms and therapeutic prospects, Medicinal research reviews. 2023; 43(3): 683-712.
14. Mou Y, Wang J, Wu J, He D, Zhang C, Duan C, et al. Ferroptosis, a new form of cell death: opportunities and challenges in cancer, Journal of hematology & oncology. 2019; 12(1): 1-16.
15. Zeng F, Nijiati S, Tang L, Ye J, Zhou Z, Chen X. Ferroptosis Detection: From Approaches to Applications, Angewandte Chemie International Edition. 2023; e202300379.
16. Xue Y, Zhang L, Liu F, Dai F, Kong L, Ma D, et al. Alkaline "Nanoswords" Coordinate Ferroptosis-like Bacterial Death for Antibiosis and Osseointegration, ACS nano. 2023; 17(3): 2711-24.
17. Liu K, Huang L, Qi S, Liu S, Xie W, Du L, et al. Ferroptosis: The Entanglement between Traditional Drugs and Nanodrugs in Tumor Therapy, Advanced Healthcare Materials. 2023; 2203085.
18. Chen C, Du W, Jing W, Sun P, Shi C, Zhang S, et al. Leveraging tumor cell ferroptosis for colorectal cancer treatment via nanoelicitor-activated tumoricidal immunity, Chemical Engineering Journal. 2022; 430: 132983.
19. Xu X, Chen Y, Gui J, Liu P, Huang Y, Shao B, et al. A biomimetic nanodrug self-assembled from small molecules for enhanced ferroptosis therapy, Biomaterials Science. 2022; 10(3): 770-80.
20. Wang Y, Chen Q, Song H, Zhang Y, Chen H, Liu P, et al. A Triple Therapeutic Strategy with Antiexosomal Iron Efflux for Enhanced Ferroptosis Therapy and Immunotherapy. Small. 2022; 18(41): 2201704.
21. Li F, Wu X, Liu H, Liu M, Yue Z, Wu Z, et al. Copper Depletion Strongly Enhances Ferroptosis via Mitochondrial Perturbation and Reduction in Antioxidative Mechanisms, Antioxidants. 2022; 11(11): 2084.
22. Wang WJ, Ling YY, Zhong YM, Li ZY, Tan CP, Mao ZW. Ferroptosis-enhanced cancer immunity by a ferrocene-appended iridium (III) Diphosphine complex, Angewandte Chemie. 2022; 134(16): e202115247.
23. Hu R, Dai C, Dai X, Dong C, Huang H, Song X, et al. Topology regulation of nanomedicine for autophagy-augmented ferroptosis and cancer immunotherapy. Science Bulletin. 2023; 68(1): 77-94.
24. Yao Y, Cai X, Fei W, Ye Y, Zhao M, Zheng C. The role of short-chain fatty acids in immunity, inflammation and metabolism, Critical reviews in food science and nutrition. 2022; 62(1): 1-12.
25. Yan J, Pan Y, Shao W, Wang C, Wang R, He Y, et al. Beneficial effect of the short-chain fatty acid propionate on vascular calcification through intestinal microbiota remodelling, Microbiome. 2022; 10(1): 1-30.
26. Sanna S, van Zuydam NR, Mahajan A, Kurilshikov A, Vich Vila A, Võsa U, et al. Causal relationships among the gut microbiome, short-chain fatty acids and metabolic diseases, Nature genetics. 2019; 51(4): 600-5.
27. Aho VT, Houser MC, Pereira PA, Chang J, Rudi K, Paulin L, et al. Relationships of gut microbiota, short-chain fatty acids, inflammation, and the gut barrier in Parkinson's disease, Molecular Neurodegeneration. 2021; 16(1): 1-14.
28. Ikeda T, Nishida A, Yamano M, Kimura I. Short-chain fatty acid receptors and gut microbiota as therapeutic targets in metabolic, immune, and neurological diseases, Pharmacology & therapeutics. 2022; 108273.
29. Shashni B, Nagasaki Y. Short-chain fatty acid-releasing nano-prodrugs for attenuating growth and metastasis of melanoma, Acta Biomaterialia. 2023; 159: 226-36.
30. Donohoe DR, Holley D, Collins LB, Montgomery SA, Whitmore

AC, Hillhouse A, et al. A Gnotobiotic Mouse Model Demonstrates That Dietary Fiber Protects against Colorectal Tumorigenesis in a Microbiota-and Butyrate-Dependent MannerFiber–Microbiota–Butyrate Axis in Tumor Suppression, Cancer discovery. 2014; 4(12): 1387-97.

31. Hajjar R, Richard CS, Santos MM. The role of butyrate in surgical and oncological outcomes in colorectal cancer, American Journal of Physiology-Gastrointestinal and Liver Physiology. 2021; 320(4): G601-8.
32. Okumura S, Konishi Y, Narukawa Y, Sugiura Y, Yoshimoto S, Arai Y, et al. Gut bacteria identified in colorectal cancer patients promote tumourigenesis via butyrate secretion, Nature communications. 2021; 12(1): 5674.
33. Dmitrieva-Posocco O, Wong AC, Lundgren P, Golos AM, Descamps HC, Dohnalová L, et al. β-Hydroxybutyrate suppresses colorectal cancer. Nature. 2022; 605(7908): 160-5.
34. Xie Y, Hou W, Song X, Yu Y, Huang J, Sun X, et al. Ferroptosis: process and function, Cell Death & Differentiation. 2016; 23(3): 369-79.
35. Nishizawa H, Matsumoto M, Shindo T, Saigusa D, Kato H, Suzuki K, et al. Ferroptosis is controlled by the coordinated transcriptional regulation of glutathione and labile iron metabolism by the transcription factor BACH1, The Journal of Biological Chemistry. 2019; 295: 69-82.
36. Yang WS, Sriramaratnam R, Welsch ME, Shimada K, Skouta R, Viswanathan VS, et al. Regulation of Ferroptotic Cancer Cell Death by GPX4. Cell. 2014; 156(1-2): 317-31.